QSM of Substantia Nigra and Improved Characterization of Substantia Nigra

Jason Langley[1], Daniel E Huddleston[2], Nishant Zachariah[3], Xiangchuan Chen[1], and Xiaoping Hu[1]

[1]*Wallace H. Coulter Department of Biomedical Engineering, Emory University and Georgia Institute of Technology, Atlanta, GA, United States,* [2]*Center for Health Research, Southeast, Kaiser Permanente, Atlanta, GA, United States,* [3]*Department of Electrical and Computer Engineering, Georgia Institute of Technology, Atlanta, GA, United States*

AUDIENCE: Researchers interested in imaging iron and neuromelanin changes in the substantia nigra.

PURPOSE

The substantia nigra (SN) is comprised of two sub-regions, the SN pars compacta and SN pars reticulata. The pars compacta contains high levels of neuromelanin (NM) while the pars reticulate contains high levels of iron. Delineation of the SN has focused on generating NM-sensitive contrast in the SN using magnetization transfer (MT) effects [1-3] or imaging iron stores in the SN using either 1) susceptibility weighted imaging (SWI) or 2) quantitative susceptibility mapping (QSM) [4]. A recent report [5] highlighted spatial and morphological incongruence of SN volumes estimated using MT-based NM sensitive MRI (NM-MRI) and SWI (incongruence illustrated in Fig. 1). However, in [5] phase was used to estimate iron content and there are conflicting accounts as to the accuracy of phase as a measure of iron content. This abstract applies a more quantitative approach, QSM, for estimation of iron and further characterizes the spatial and contrast incongruence seen in the SN from NM-MRI and SWI.

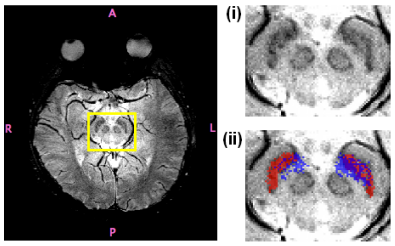

Fig. 1. An axial view of the SWI image (left) with MTC and SWI SN volumes shown in blue and red in (ii), respectively.

METHODS

Data Acquisition: All experiments were performed on a 3 T scanner (Tim TRIO, Siemens Medical Solutions, Malvern, PA) using a 12 channel transmit / receive coil. Seven normal volunteers participated in this study after obtaining informed consent in accordance with our institutional review board regulations. A three-dimensional dual echo gradient echo sequence with the following parameters was used to acquire the data: $TE_1/TE_2/TR$=2.68/20/337 ms, 64 contiguous slices, 384×312 imaging matrix, 162×200 mm (0.7×0.7×0.7 mm), 7 repetitions, flip angle (FA)=40°, MTC pulse (500°, 1.2 kHz off-resonance, 10 ms duration), and 470 Hz/pixel receiver bandwidth.

MTC Image Processing: Magnitude data of TE_1 was averaged over all repetitions after spatial registration to the first measurement using FLIRT in the FSL software package (Oxford University, United Kingdom). The SN was segmented from the averaged image using the method presented in [3].

SWI Image Processing: Magnitude images of TE_2 were also averaged for all repetitions after spatial registration using FLIRT with the transformation matrices stored by the earlier MTC registration. Next, the phase data of TE_2 of each repetition was unwrapped [6] and the unwrapped phase maps were averaged after registration to the first measurement using the earlier stored transformation matrices. The resulting unwrapped phase map was high pass filtered, and used to generate phase mask, and susceptibility weighted images were created by multiplying the phase mask with the averaged structural image [7]. Phase unwrapping and filtering were performed using MATLAB. The SN in SWI images were segmented using the method presented in [5].

QSM Image Processing: External field contributions were removed from the unwrapped phase maps using the projection onto background fields (PDF) algorithm [8]. Next, field inversion was performed using the morphology enabled dipole inversion (MEDI) algorithm [9]. Finally susceptibility maps were normalized to the inferior longitudinal fasciculus.

Estimation of R_2* and Magnetization Transfer Contrast: Magnetization transfer contrast (MTC) and R_2* were estimated using the following equations:

$$MTC = \left|I_{SN} - I_{REF}\right| / I_{REF} \quad \text{and} \quad R_2^* = -(\log_e S(TE_2) - \log_e S(TE_1)) / \Delta TE \qquad (1)$$

where I_{SN} and I_{REF} denote the mean signal intensity in the SN and a reference region from the first echo (MT-based NM-MRI).

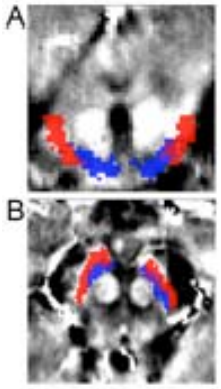

Fig. 2. *Coronal (A) and axial (B) views of the QSM map with the NM-MRI SN volume (blue) and SWI SN volume (red) overlaid.*

RESULTS AND DISCUSSION

Both contrasts show similar SN volumes (NM-MRI: 494.3±134.3 mm^3; SWI: 555.7±149.3 mm^3, p=0.28). However, the volumes had a low overlap (overlap: 5.5%±1.1%). Furthermore, if we consider each hemisphere separately, the average distance between the centers of mass (COM) for the two volumes was 6.33±0.95 mm and 6.03±0.64 mm for the left and right hemispheres, respectively. The mean MTC values for the SN volumes derived from the two contrasts were 0.016±0.03 and 0.08±0.03 (p=0.006) for the NM-MRI and SWI SN volumes, respectively and are shown in Fig. 3c. The mean susceptibility values are displayed in Fig. 3a (NM-MRI: 0.03±0.01 ppm; SWI: 0.07±0.02 ppm; p = 0.014) and the mean relaxation rates are shown in Fig. 3b (NM-MRI: 24.6±3.5 s^{-1}; SWI: 29.9±4.0 s^{-1}; p=0.046). Since both susceptibility and R_2* are sensitive to iron, we are able to infer that the SWI SN volume contains a higher iron content than the NM-MRI SN volume.

The differing contrast characteristics indicate the SN volumes seen in the two contrasts are comprised of different types of tissue. In the current protocol, two echoes were used to estimate R_2* and in the QSM procedure. Additional echoes will increase the accuracy of R_2* and susceptibility estimates. Another benefit of this approach is that both images are acquired in the same acquisition and any errors caused by inter-scan motion are removed.

CONCLUSION

We found statistically significant differences in MTC, R_2*, and susceptibility in SN volumes extracted from SWI and NM-MRI images. The presented approach is beneficial in that it offers a comprehensive approach for imaging the SN. Additional benefits arise from the sensitivity to NM, inherent to MT effects, and iron content, inherent in the phase map and corresponding susceptibility map. Furthermore, the sequence can be used to simultaneously study both iron deposition and NM degeneration in the SN from Parkinson's disease.

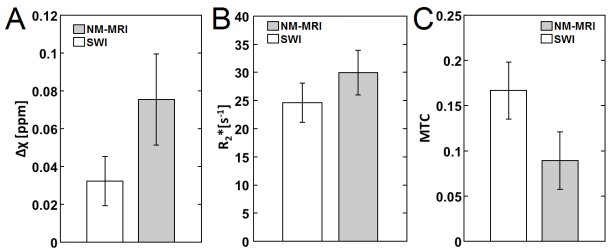

Fig. 3. Comparison of Δχ (shown in A), R_2 (shown in B), and MTC (shown in C) for NM and SWI SN volumes. Statistically significant differences are seen for all three metrics.*

REFERENCES: [1] Sasaki, *et al*. NeuroReport 17:1215 (2006); [2] Schwarz, *et al*. Movement Disorders 26:1633 (2011); [3] Chen, *et al*. MRI 32:1301-1306 (2014); [4] Lotfipour, *et al*. JMRI 35:48 (2012); [5] Langley, *et al*. Proc ISMRM 2014 #573; [6] Langley, *et al*. MRI 27:1293 (2009); [7] Haacke, *et al*. MRM 52:612 (2004); [8] Liu, *et al*. NMR Biomed 24:1129; [9] Liu, *et al*. MRM 66:777 (2011)

ACKNOWLEDGEMENTS: This work was partially funded by William N. and Bernice E. Bumpus Foundation Early Career Investigator Innovation Award (BFIA 2011.3)